Electrochimica Acta 55 (2009) 383–394

Contents lists available at ScienceDirect

Electrochimica Acta

journal homepage: www.elsevier.com/locate/electacta

Synchronization of electrochemical oscillators of S-NDR type

Adrian Bîrzu[a], Vilmos Gáspár[b,*]

[a] Department of Physical and Theoretical Chemistry, University "Al. I. Cuza", Carol I bvd. no. 11, 700506 Iaşi, Romania
[b] Institute of Physical Chemistry, University of Debrecen, H-4010 Debrecen, P.O. Box 7, Hungary

ARTICLE INFO

Article history:
Received 10 November 2008
Received in revised form 18 December 2008
Accepted 23 December 2008
Available online 22 January 2009

Keywords:
Zn electrodeposition
Electrochemical oscillators
Global coupling
Synchronization
Order parameter

ABSTRACT

Electrochemical oscillators are classified as truly potentiostatic or Negative Differential Resistance (NDR) type considering, respectively, the nonessential or essential role of double-layer potential on the dynamics. NDR type oscillators are further grouped into N-NDR and S-NDR type systems where N and S refer to the characteristic shape of the polarization curve. Here, we report on the effect of global coupling on the dynamics of interacting electrochemical oscillators of S-NDR type where the electrode potential acts as an essential negative feedback variable. The Lee–Jorné scheme has been applied to model Zn electrodeposition on two or an array of 128 globally coupled nonidentical electrodes. The strength of global coupling between the electrodes can be systematically varied by changing collective and individual resistors in the circuit. Several different scenarios for synchronization and partial synchronization have been observed and analyzed. The collective dynamics is characterized by an order parameter, the average phase shift between the oscillators, and phase portraits based on Hilbert transform. The effect of changing the double-layer capacitance on the dynamics is also explored.

1. Introduction

Collective behaviour of many coupled dynamical systems is of great interest in a variety of fields including physics, chemistry, biology, etc. [1,2] Starting with the work of Kuramoto [3] and Winfree [4], there has been an ever growing interest in synchrony of globally coupled limit cycle oscillators. The theory [5] predicts the emergence of coherent dynamics above a critical value of the coupling strength. An excellent review on 25 years of research on the Kuramoto model and on the onset of synchronization in population of coupled oscillators has been written by Strogatz [6].

Experiments on a large population of electrochemical oscillators have been reported recently by Kiss et al. [7]. Electrochemical oscillators are classified as truly potentiostatic or Negative Differential Resistance (NDR) type considering, respectively, the nonessential or essential role of double-layer potential on the dynamics. NDR type oscillators are further grouped into N-NDR and S-NDR type systems where N and S refer to the characteristic shape of the polarization curve [8,9]. Kiss et al. [7,10] studied the effect of global coupling on the dynamics of interacting electrochemical oscillators of N-NDR type (electrodissolution of Ni) where the double-layer potential acts as a positive feedback variable. Here, we report on the effect of global coupling on the dynamics of interacting electrochemical oscillators of S-NDR type where the electrode potential acts as an essential negative feedback variable. The Lee–Jorné scheme [11] has been applied to model Zn electrodeposition on two or an array of 128 globally coupled electrodes. Because of surface heterogeneities, the reacting sites are inherently different in most electrochemical systems. The effect of such differences will be considered by modelling nonidentical electrodes.

The collective dynamics of two and 128 globally coupled nonidentical electrodes will be studied by systematically varying the strength of global coupling between the electrodes. Synchronization will be characterized by an order parameter and the average phase shift between two oscillators, while the dynamics of the array of oscillators is characterized by an average order parameter, phase distribution plots and phase portraits based on Hilbert transform of the individual currents of the coupled electrodes.

2. Models and methods

2.1. Model of Zn electrodeposition

The Lee–Jorné model [11] defining the rate of change in the fractional coverage $0 \le \theta_1 \le 1$ and $0 \le \theta_2 \le 1$ by the adsorbed H_{ad} and Zn_{ad}^{+} on the electrode surface, respectively, has been applied to simulate the dynamics of Zn electrodeposition. The model is based

* Corresponding author. Tel.: +36 52 512 900x22389; fax: +36 52 512915.
E-mail address: gasparv@delfin.unideb.hu (V. Gáspár).

0013-4686/$ – see front matter © 2009 Elsevier Ltd. All rights reserved.
doi:10.1016/j.electacta.2009.01.041

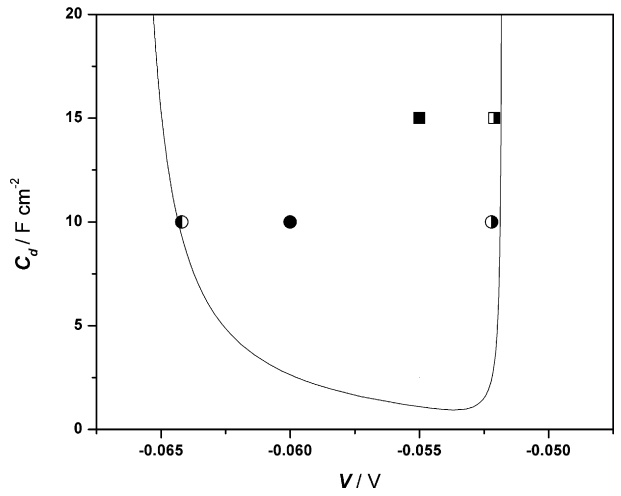

Fig. 1. Bifurcation diagram of the Lee–Jorné model for Zn electrodeposition. Solid curve shows the locus of Hopf bifurcation in the specific double-layer capacitance C_d (F cm^{-2}) *vs.* circuit potential V (V) parameter space at other parameter values as defined in the text. Symbols identify the special points where synchronization of two and an array of 128 electrodes has been studied: P1 (◐): $V = -0.0642$ V, $C_d = 10$ F cm^{-2}; P2 (●): $V = -0.06$ V, $C_d = 10$ F cm^{-2}; P3 (◑): $V = -0.0522$ V, $C_d = 10$ F cm^{-2}; P4 (■): $V = -0.055$ V, $C_d = 15$ F cm^{-2}; P5 (◨): $V = -0.0521$ V, $C_d = 15$ F cm^{-2}.

on the following reaction scheme:

$$\begin{aligned}
&H^+ + e^- \xrightarrow{A_1} H_{ad}\\
&H^+ + H_{ad} + e^- \xrightarrow{A_2} H_2\\
&Zn^{2+} + Zn_{ad}{}^+ + e^- \underset{A'_3}{\overset{A_3}{\rightleftharpoons}} 2Zn_{ad}{}^+\\
&Zn_{ad}{}^+ + H_{ad} \xrightarrow{A_4} H^+ + Zn\\
&Zn_{ad}{}^+ + e^- \xrightarrow{A_5} Zn\\
&Zn^{2+} + H_{ad} \xrightarrow{A_6} Zn_{ad}{}^+ + H^+
\end{aligned} \tag{1}$$

Notice that the forward reaction of the third step is autocatalytic which introduces a positive feedback to the system. On the other hand, it is well known [8] that in S-NDR type electrochemical systems the double-layer potential e acts as a negative feedback variable. The interplay of the two feedbacks may then lead to current oscillations. When Zn electrodeposition is carried out under potentiostatic condition at a fixed circuit potential V, by considering the local charge balance at the double-layer and the IR drop in the electrolyte and an external resistor in series with the electrode (total resistance R), the evolution of the dynamical variables e, θ_1 and θ_2 can be described by the following differential equations:

$$C_d \frac{de}{dt} = \frac{V - e}{AR} - j_F(e, \theta_1, \theta_2) \tag{2}$$

$$\Gamma_1 \frac{d\theta_1}{dt} = A_1(1 - \theta_1 - \theta_2) - A_2\theta_1 - A_4\theta_1\theta_2 - A_6\theta_1 \tag{3}$$

$$\Gamma_2 \frac{d\theta_2}{dt} = A_3\theta_2(1 - \theta_1 - \theta_2) - A'_3\theta_2^2 - A_4\theta_1\theta_2 - A_5\theta_2 + A_6\theta_1 \tag{4}$$

where C_d (F cm^{-2}) is the specific double layer capacitance, while Γ_1 and Γ_2 (mol cm^{-2}) are the maximal surface capacities for H_{ad} and $Zn_{ad}{}^+$, respectively. Their values were approximated by Epelboin et al. [12,13] from impedance measurements: $\Gamma_1 = 1.36 \times 10^{-7}$ mol cm^{-2}, $\Gamma_2 = 9.067 \times 10^{-11}$ mol cm^{-2}. The Faradaic current density j_F is defined as

$$\begin{aligned}
&j_F(e, \theta_1, \theta_2)\\
&\quad = F\left[-A_1(1 - \theta_1 - \theta_2) - A_2\theta_1 - A_3\theta_2(1 - \theta_1 - \theta_2) + A'_3\theta_2^2 - A_5\theta_2\right]
\end{aligned} \tag{5}$$

where F is the Faradaic constant and $A_1, \ldots, A_6$ (mol cm^{-2} s^{-1}) are kinetic parameters. Their values were optimized by Lee and Jorné [11]:

$$\begin{aligned}
&A_1 = 5.53 \times 10^{-7} \exp(-19.3\, e) \text{ mol cm}^{-2}\text{ s}^{-1},\\
&A_2 = 3 \times 10^{-9} \exp(-29.3\, e) \text{ mol cm}^{-2}\text{ s}^{-1},\\
&A_3 = 2.45 \times 10^{-5} \exp(-33.8\, e) \text{ mol cm}^{-2}\text{ s}^{-1},\\
&A'_3 = 7.5 \times 10^{-5} \exp(4.8\, e) \text{ mol cm}^{-2}\text{ s}^{-1},\\
&A_4 = 1.0 \times 10^{-6} \text{ mol cm}^{-2}\text{ s}^{-1},\\
&A_5 = 5.4 \times 10^{-8} \exp(-38.6\, e) \text{ mol cm}^{-2}\text{ s}^{-1}, \text{ and}\\
&A_6 = 1.0 \times 10^{-9} \text{ mol cm}^{-2}\text{ s}^{-1}.
\end{aligned}$$

Notice that for those steps of reaction scheme (1) in which electron e^- uptake is indicated, the kinetic parameters are given as exponential functions of the double-layer potential. These nonlinear functions also contribute to the nonlinearity of the system resulting in an S-shaped polarization curve always characteristic of an S-NDR type system. For simplicity, we assume unit surface area ($A = 1$ cm^2) for each electrode in all reported calculations.

Fig. 1 shows the bifurcation diagram of the Lee–Jorné model defined by Eqs. (2)–(5) in the specific double-layer capacitance C_d (F cm^{-2}) *vs.* circuit potential V (V) parameter space at $R = 2\ \Omega$ and other parameter values as defined above. The solid curve shows the locus of Hopf bifurcation where current oscillations appear or disappear. Since the high values of specific double layer capacitance shown in the figure are quite unrealistic for an experimental system, spontaneous current oscillations would never occur during cathodic Zn electrodeposition. However, Kiss

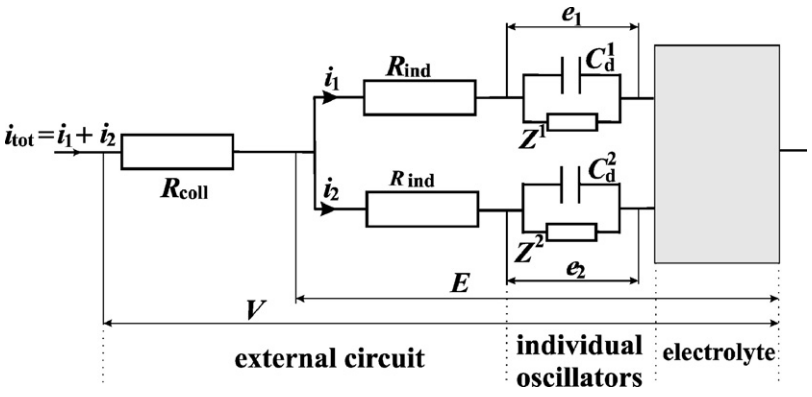

Fig. 2. Equivalent electric circuit of two globally coupled electrochemical oscillators.

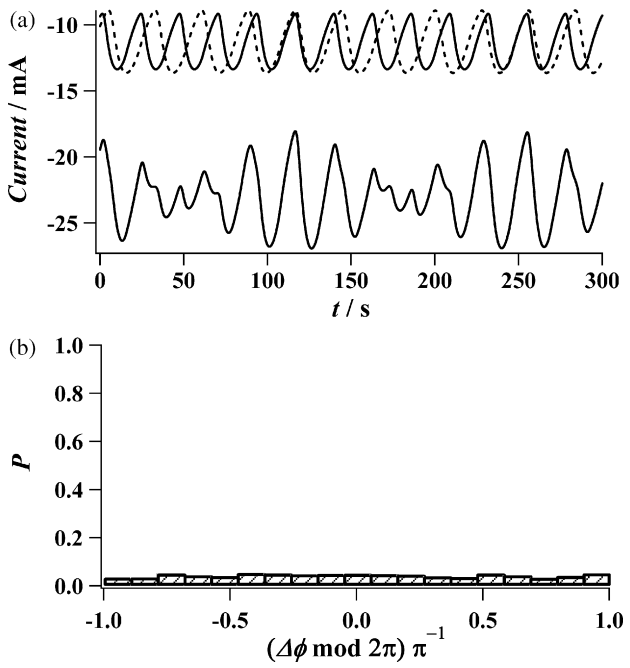

Fig. 3. Unsynchronized oscillations of two uncoupled oscillators ($\kappa = 0\ \Omega^{-1}\ cm^{-2}$) at parameters corresponding to reference point P1 (◐) in Fig. 1. The electrodes have been made nonidentical as described in the text. (a) Time series of the individual currents (upper part, continuous line i_1, dashed line i_2) and of the total current i_{tot} (lower part, continuous line). (b) Histogram of the probability of different phase shift values between the two oscillators (resolution 0.1π).

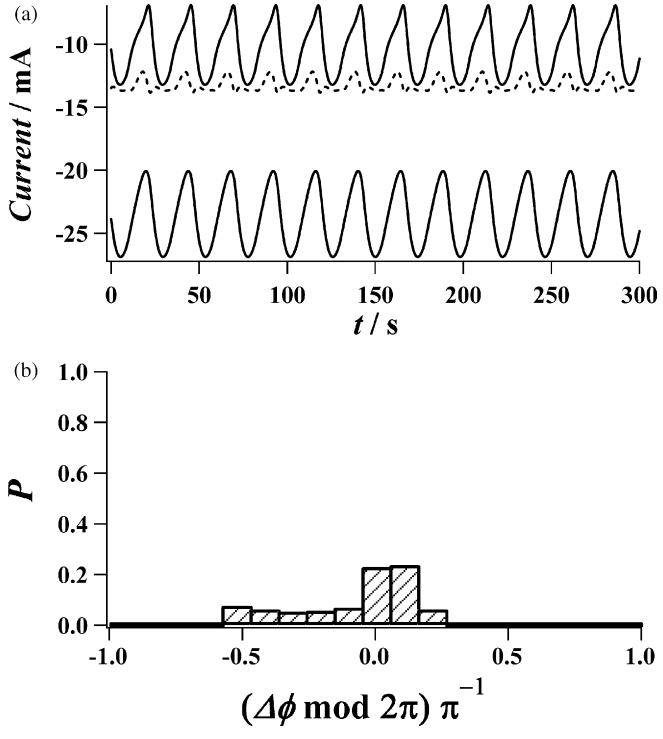

Fig. 4. Synchronized in-phase oscillations at $\kappa = 0.8\ \Omega^{-1}\ cm^{-2}$ of two nonidentical oscillators as defined in Fig. 3. (a) Time series of the current of the individual electrodes (upper part, continuous line i_1, dashed line i_2) and of the total current i_{tot} (lower part, continuous line). (b) Histogram of the probability of different phase shift values between the two oscillators (resolution 0.1π).

et al. [14] have recently shown that by applying a so called "differential controller" one can easily modify the time-scale constant of variable e. The effect of this special feedback algorithm is equal to formally adding a pseudo double-layer capacitance to the inherent double-layer capacitance of the electrode. Indeed, by using the differential controller such that pseudo double-layer capacitance had been generated in the order of few Farads, Kiss et al. [14] were able to experimentally induce current oscillations during cathodic Zn electrodeposition under potentiostatic condition.

Symbols in Fig. 1 identify some special points in the bifurcation diagram where calculations have been performed to study and characterize the synchronization of two or an array of 128 globally coupled nonidentical Zn electrodes. The autonomous oscillations at points P1 and P2 are periodic, almost harmonic, while at P3 to P5 they are periodic and relaxation type.

2.2. Model of two globally coupled Zn electrodes

Fig. 2 shows the equivalent electric circuit of two globally coupled Zn electrodes. R_{ind} is an individual external resistance in series with an electrode. The electrode itself is considered as an oscillator composed of a capacitance and an 'impedance' in parallel. R_{coll} is a collective (external) resistance including solution resistance. V is the total voltage applied under potentiostatic control. E is the actual total potential acting on the coupled system, while e_1 and e_2 are double-layer potential values of electrode 1 and 2, respectively.

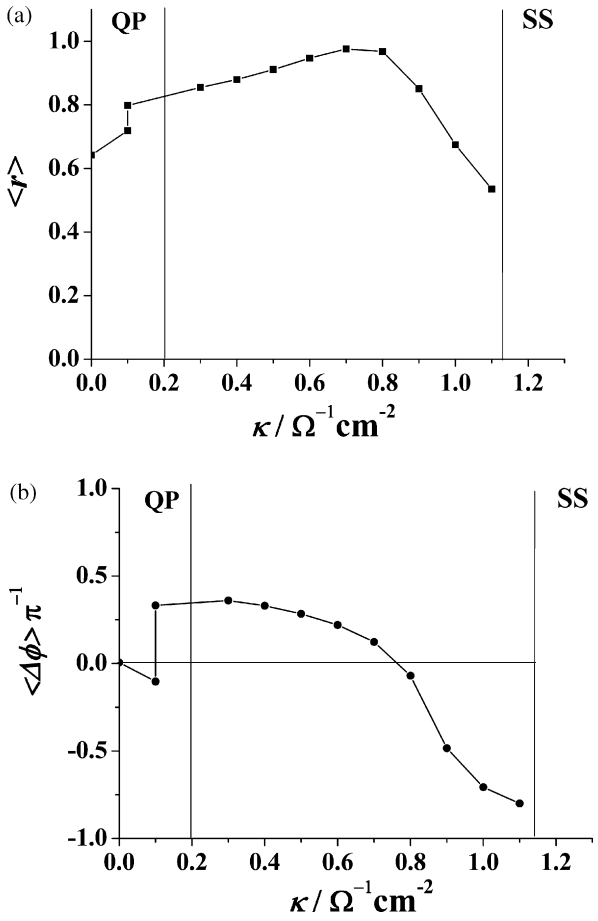

Fig. 5. Characterizing the collective dynamics of two globally coupled electrochemical oscillators defined in Fig. 3. (a) Average order parameter $\langle r \rangle$ and (b) average phase shift $\langle \Delta\varphi \rangle / \pi$ between the two oscillators as a function of the coupling strength κ.

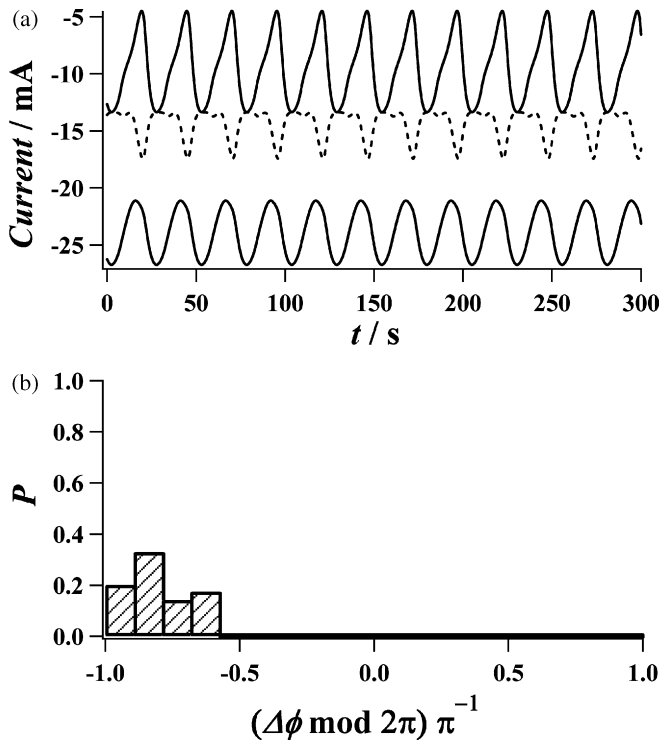

Fig. 6. Synchronized anti-phase oscillations at $\kappa = 1.1\ \Omega^{-1}\,\mathrm{cm}^{-2}$ of two nonidentical oscillators as defined in Fig. 3. (a) Time series of the current of the individual electrodes (upper part, continuous line i_1, dashed line i_2) and of the total current i_{tot} (lower part, continuous line). (b) Histogram of the probability of different phase shift values between the two oscillators (resolution 0.1π).

The total current i_{tot} is the sum of the individual currents i_1 and i_2.

By considering the local charge balances and the IR-drop through the collective and individual resistors, the differential equations describing the dynamic evolution of two electrochemical oscillators that are globally coupled are as follows (see Appendix A):

Electrode 1

$$C_{d,1}\frac{de_1}{dt} = \frac{V - e_1}{AR_{ekv}} - j_{F,1}(e_1, \theta_{1,1}, \theta_{2,1}) + \kappa(e_2 - e_1) \tag{6}$$

$$\Gamma_{1,1}\frac{d\theta_{1,1}}{dt} = A_{1,1}(1 - \theta_{1,1} - \theta_{2,1}) - A_{2,1}\theta_{1,1} - A_{4,1}\theta_{1,1}\theta_{2,1} - A_{6,1}\theta_{1,1} \tag{7}$$

$$\Gamma_{2,1}\frac{d\theta_{2,1}}{dt} = A_{3,1}\theta_{2,1}(1 - \theta_{1,1} - \theta_{2,1}) - A'_{3,1}\theta^2_{2,1} - A_{4,1}\theta_{1,1}\theta_{2,1} - A_{5,1}\theta_{2,1} + A_{6,1}\theta_{1,1} \tag{8}$$

Electrode 2

$$C_{d,2}\frac{de_1}{dt} = \frac{V - e_2}{AR_{ekv}} - j_{F,2}(e_2, \theta_{1,2}, \theta_{2,2}) + \kappa(e_1 - e_2) \tag{9}$$

$$\Gamma_{1,2}\frac{d\theta_{1,2}}{dt} = A_{1,2}(1 - \theta_{1,2} - \theta_{2,2}) - A_{2,2}\theta_{1,2} - A_{4,2}\theta_{1,2}\theta_{2,2} - A_{6,2}\theta_{1,2} \tag{10}$$

$$\Gamma_{2,2}\frac{d\theta_{2,2}}{dt} = A_{3,2}\theta_{2,2}(1 - \theta_{1,2} - \theta_{2,2}) - A'_{3,2}\theta^2_{2,2} - A_{4,2}\theta_{1,2}\theta_{2,2} - A_{5,2}\theta_{2,2} + A_{6,2}\theta_{1,2} \tag{11}$$

where the individual Faradaic current density $j_{F,j}$ is defined as

$$j_{F,j} = F\left[-A_{1,j}(1 - \theta_{1,j} - \theta_{2,j}) - A_{2,j}\theta_{1,j} - A_{3,j}\theta_{2,j}(1 - \theta_{1,j} - \theta_{2,j}) + A'_{3,j}\theta^2_{2,j} - A_{5,j}\theta_{2,j}\right] \tag{12}$$

Index j stands for the jth electrode ($j = 1, 2$). The kinetic parameters $A_{1,j}, \ldots, A_{6,j}$ for both electrodes are calculated as earlier but by considering the actual value of the double layer potential of the jth electrode (e_1 and e_2). The two electrodes were made nonidentical by decreasing (for electrode 1) and increasing (for electrode 2) the earlier defined maximal surface capacity values by 25% as follows: electrode 1: $\Gamma_{1,1} = 1.02 \times 10^{-7}\ \mathrm{mol\,cm^{-2}}$, $\Gamma_{2,1} = 6.80 \times 10^{-11}\ \mathrm{mol\,cm^{-2}}$; electrode 2: $\Gamma_{1,2} = 1.70 \times 10^{-7}\ \mathrm{mol\,cm^{-2}}$, $\Gamma_{2,2} = 1.13 \times 10^{-10}\ \mathrm{mol\,cm^{-2}}$. As derived in Appendix A, $R_{ekv} = 2R_{coll} + R_{ind}(\Omega)$, and $\kappa = (\kappa_2/A) > 0$ ($\Omega\,\mathrm{cm}^{-2}$) is a constant defining the strength of coupling:

$$\kappa = \frac{1}{A}\left(\frac{R_{coll}}{R_{ind}}\frac{1}{R_{ekv}}\right) \tag{13}$$

Dynamics of the two globally coupled Zn electrodes has been explored by systematically varying the coupling strength κ at

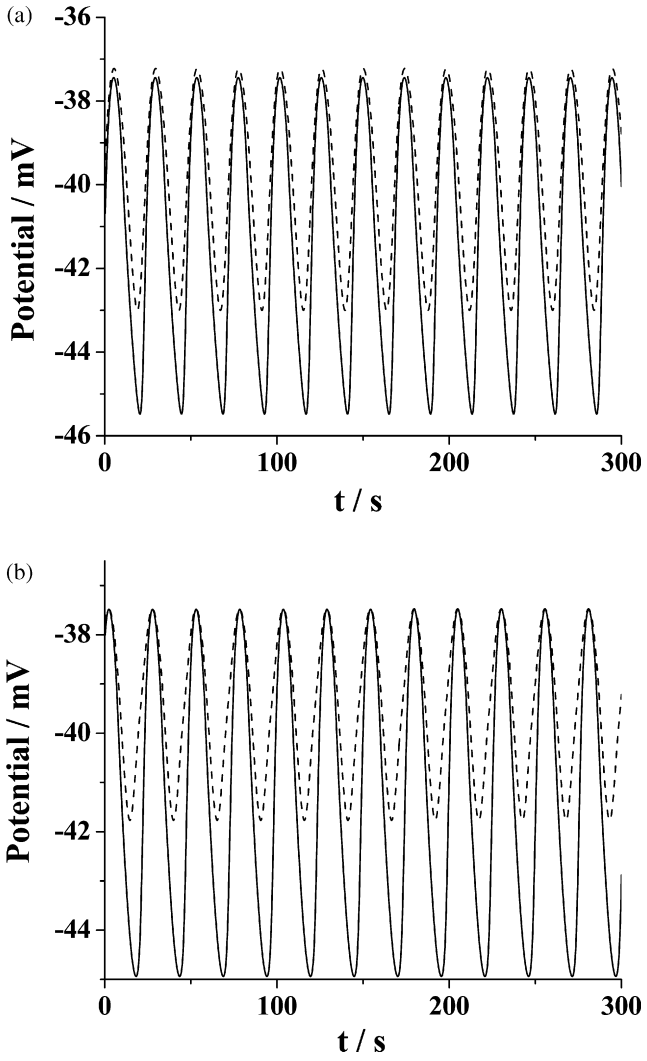

Fig. 7. Time series of the individual double-layer potential values (continuous line e_1, dashed line e_2) of two globally coupled nonidentical electrodes in case of (a) synchronized in-phase (Fig. 4) and (b) anti-phase current oscillations (Fig. 6).

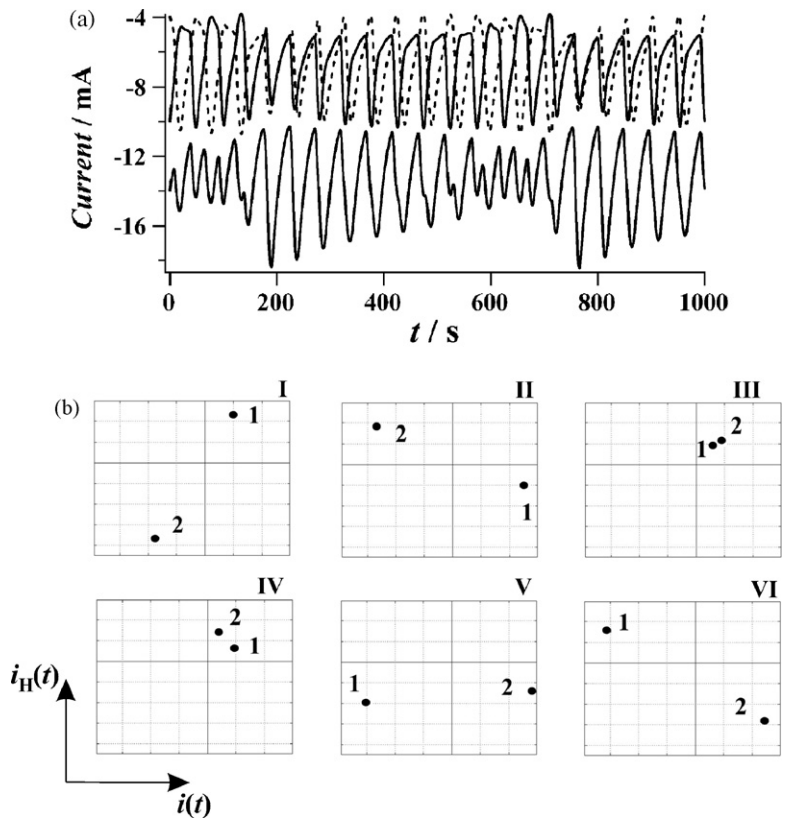

Fig. 8. Partial synchronization of two nonidentical oscillators at $\kappa = 0.2\ \Omega^{-1}\ cm^{-2}$ and at other parameters corresponding to reference point P4 (■) in Fig. 1. (a) Time series of the current of the individual electrodes (upper part, continuous line i_1, dashed line i_2) and of the total current i_{tot} (lower part, continuous line). (b) Phase portraits for the two coupled oscillators for $t = 12.5$ s (I), 81.8 s (II), 209.7 s (III), 257.6 s (IV), 325.9 (V) and 477.3 s (VI).

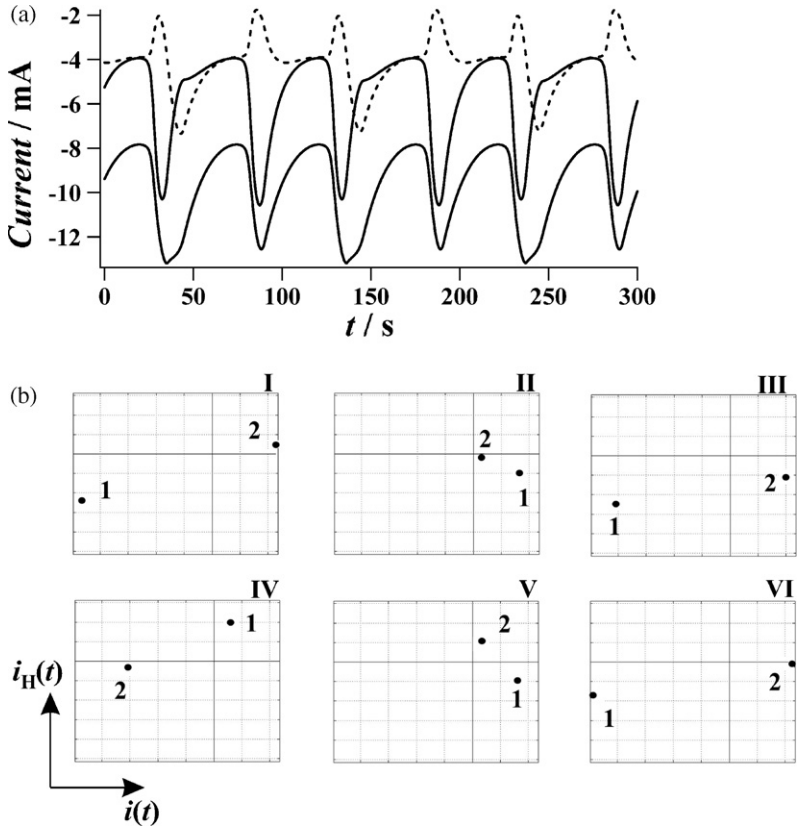

Fig. 9. Period-2 synchronization at $\kappa = 0.5\ \Omega^{-1}\ cm^{-2}$ and at other parameters corresponding to reference point P3 (◑) in Fig. 1. (a) Time series of the current of the individual electrodes (upper part, continuous line i_1, dashed line i_2) and of the total current i_{tot} (lower part, continuous line). (b) Phase portraits for the two coupled oscillators for $t = 87.6$ s (I), 121.8 s (II), 133.5 s (III), 146.2 s (IV), 172.6 (V) and 189.2 s (VI).

different values of circuit potential V and specific double-layer capacitance C_d while holding all other parameters constant. This corresponds to an experimental procedure when one changes both R_{coll} and R_{ind} in such a way that the total external resistance $R_{tot} = R_{evk}/2$ is held constant. In all our calculations, $A = 1\,cm^2$ and $R_{ekv} = 2\,\Omega$, which is the same as that applied in calculating Fig. 1 for a single electrode.

The immediate effect of global coupling can be easily understood by taking a look at a situation when, for example, $e_2 > e_1$. According to Eq. (6) the rate in the change of the double layer potential e_1 will increase as $\kappa(e_2 - e_1) > 0$, while according to Eq. (9) the rate in the change of the double layer potential e_2 will decrease as $\kappa(e_1 - e_2) < 0$. The opposite situation $e_1 > e_2$ will result in opposite effects. In all, global coupling through the electrolyte affect the dynamics of the electrodes in such a way that the double-layer potential values tend to get closer to each other, resulting ultimately in a synchronized behaviour.

Consequently, at a first sight, a positive global coupling should act synchronizing. However, in complex oscillatory systems, the effect of a positive global coupling can be different. Thus, examples of such more involved effects can be found in [15], where galvanostatic control, i.e., a positive global coupling, can be desynchronizing in a SNDR spatially distributed electrochemical system, or [16], where a collection of different weakly positive coupled oscillators exhibit traveling wave solutions. Another report presents the case of positive coupled nonidentical oscillators, where the frequencies synchronize and the system presents 'frequency plateaus' [17]. As it will be seen from the following results, also for the system studied in the present work, the effect of a positive global coupling, in terms of synchronization, is not trivial.

By numerically integrating the system of ordinary differential equations (6)–(11) that define the dynamics of two globally coupled Zn electrodes, the current of the jth electrode is calculated as follows:

$$i_j = \frac{V - e_j}{R_{ekv}} + 2\kappa_2(\bar{e} - e_j) \tag{14}$$

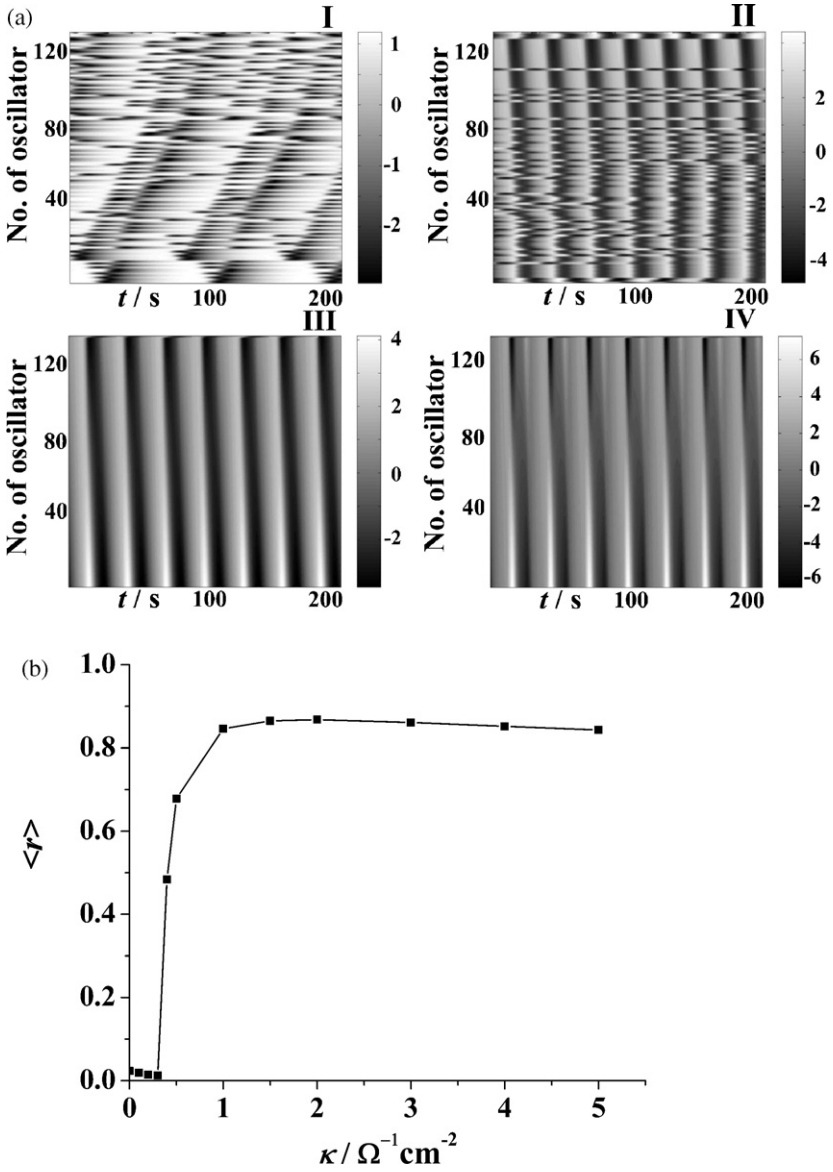

Fig. 10. Almost complete synchronization of the current oscillations of globally coupled 128 nonidentical electrodes. (a) Time evolution of the current of the individual electrodes at different values of coupling strength κ: 0 Ω^{-1} cm^{-2} (I), 0.4 Ω^{-1} cm^{-2} (II), 1.0 Ω^{-1} cm^{-2} (III) and 10.0 Ω^{-1} cm^{-2} (IV) and other parameters corresponding to reference point P2 (●) in Fig. 1. The electrodes have been made nonidentical as described in the text. The grey scale on the side of the frames scales the current values in mA. (b) The average order parameter $\langle r \rangle$ as a function of κ.

where $\bar{e} = (e_1 + e_2)/2$ is the mean of the individual double-layer potential values. The total current i_{tot} is the sum of the individual currents. Initial conditions for the integrations using the LSODE routines were chosen as $e_1(0) = 0.01$ V and $e_2(0) = -0.01$ V, while all $0 \leq \theta\ (0) \leq 1$ values were generated by a random number generator. All time series data have been collected and used for other calculations after long enough transient periods (generally 1000 s).

2.3. Model of an array of n globally coupled Zn electrodes

The differential equations describing the dynamic evolution of the kth electrode ($k = 1,\ldots, n$) in an array of n globally coupled Zn electrodes are (see Appendix B):

$$C_{d,k}\frac{de_k}{dt} = \frac{V - e_k}{AR_{ekv}} - j_{F,k}(e_k, \theta_{1,k}, \theta_{2,k}) + \kappa(\bar{e} - e_k) \tag{15}$$

$$\Gamma_{1,k}\frac{d\theta_{1,k}}{dt} = A_{1,k}(1 - \theta_{1,k} - \theta_{2,k}) - A_{2,k}\theta_{1,k} - A_{4,k}\theta_{1,k}\theta_{2,k} - A_{6,k}\theta_{1,k} \tag{16}$$

$$\Gamma_{2,k}\frac{d\theta_{2,k}}{dt} = A_{3,k}\theta_{2,k}(1 - \theta_{1,k} - \theta_{2,k}) - A'_{3,k}\theta^2_{2,k} - A_{4,k}\theta_{1,k}\theta_{2,k} - A_{5,k}\theta_{2,k} + A_{6,k}\theta_{1,k} \tag{17}$$

where the individual Faradaic current density $j_{F,k}$ is defined as

$$j_{F,k} = F\left[-A_{1,k}(1 - \theta_{1,k} - \theta_{2,k}) - A_{2,k}\theta_{1,k} - A_{3,k}\theta_{2,k}(1 - \theta_{1,k} - \theta_{2,k}) + A'_{3,k}\theta^2_{2,k} - A_{5,k}\theta_{2,k}\right] \tag{18}$$

and $\bar{e} = (1/n)\sum_{k=1}^{n} e_k$ is the mean of the individual double-layer potential values. The kinetic parameters $A_{1,k},\ldots, A_{6,k}$ for each electrode are calculated as earlier but by considering the actual value of the double layer potential of the kth electrode (e_k).

The electrodes were made nonidentical by setting the maximal surface capacity values according to the following formulas

$$\Gamma_{1,k} = \Gamma_{1,low} + (k-1)\frac{\Gamma_{1,high} - \Gamma_{1,low}}{n-1}, \quad k = 1,\ldots, n$$
$$\Gamma_{2,k} = \Gamma_{2,low} + (k-1)\frac{\Gamma_{2,high} - \Gamma_{2,low}}{n-1}, \quad k = 1,\ldots, n \tag{19}$$

$\Gamma_{1,low} = 1.02 \times 10^{-7}$ mol cm^{-2}, $\Gamma_{1,high} = 1.70 \times 10^{-7}$ mol cm^{-2} and $\Gamma_{2,low} = 6.80 \times 10^{-11}$ mol cm^{-2}, $\Gamma_{2,high} = 1.13 \times 10^{-10}$ mol cm^{-2} are the values used for electrode 1 and electrode 2, respectively, in the coupled system of two nonidentical electrodes. As derived in Appendix B, $R_{ekv} = nR_{coll} + R_{ind}(\Omega)$, and $\kappa = (\kappa_n/A) > 0$ (Ω cm^{-2}) is a constant defining the strength of coupling:

$$\kappa = \frac{1}{A}\left(\frac{nR_{coll}}{R_{ind}}\frac{1}{R_{ekv}}\right) \tag{20}$$

Dynamics of $n = 128$ globally coupled Zn electrodes has been explored again by systematically varying the coupling strength κ at different values of circuit potential V and specific double-layer capacitance C_d while holding all other parameters constant. As before, for all calculations $A = 1$ cm^2 and $R_{ekv} = 2\ \Omega$ were used. As long as only the global coupling between the oscillators is considered, their geometrical arrangement in a corresponding experimental implementation would have no importance upon

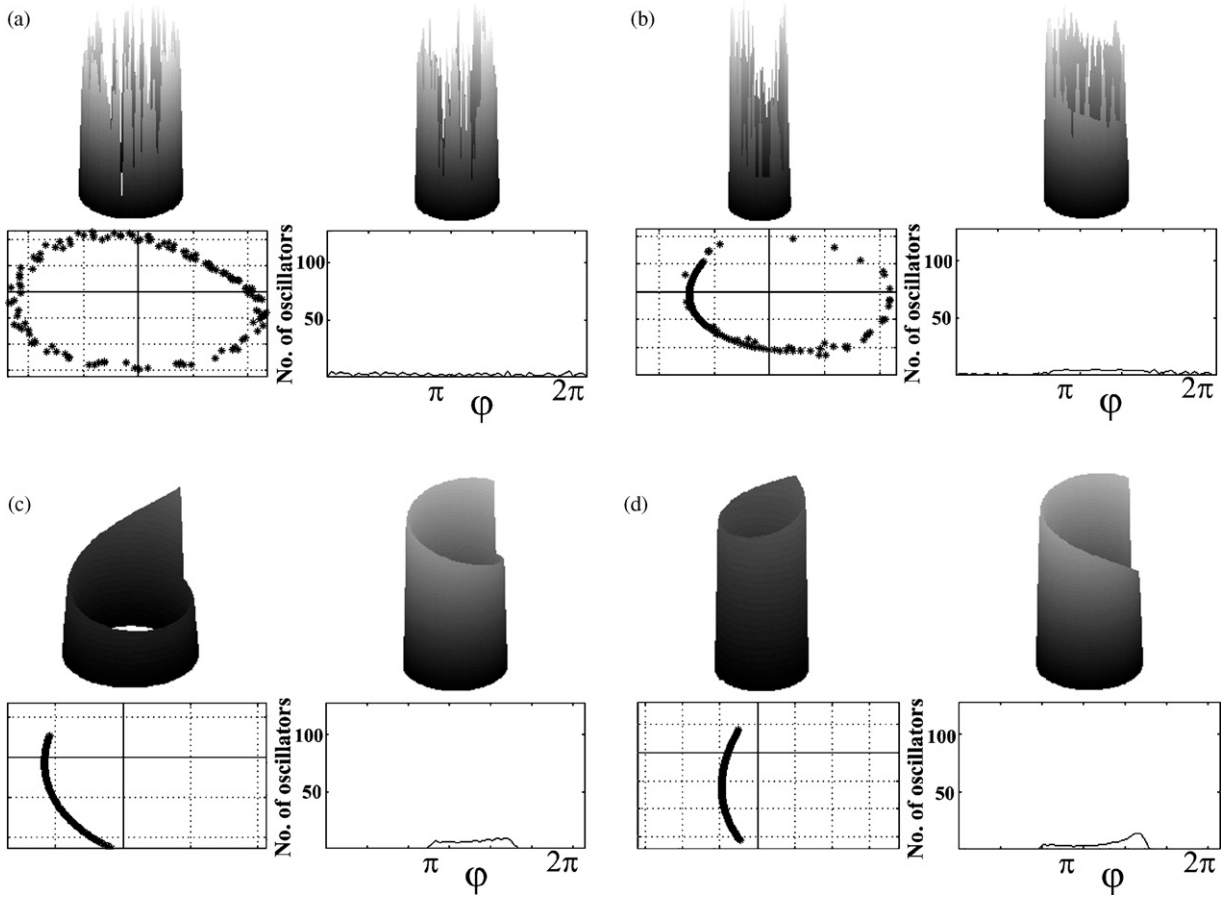

Fig. 11. Dynamics of 128 coupled oscillators showing almost complete synchronization (Fig. 10). In each frame (a)–(d): upper left – current of the individual oscillators; upper right – instantaneous phase of the individual oscillators; lower left – a characteristic phase portrait; lower right – distribution of instantaneous phase of the individual oscillators. Frames (a), (b), (c) and (d) correspond, respectively, to the state of the system at $t = 12.45$ s of the grey scale figures (I), (II), (III) and (IV) in Fig. 10a.

the dynamics. The effect of global coupling can be explained by looking at a situation when, for example, $\bar{e} > e_k$. According to Eq. (15) the rate in the change of the double layer potential e_k will increase as $\kappa(\bar{e} - e_k) > 0$. The opposite situation $e_k > \bar{e}$ results in the opposite effect. In all, global coupling through the electrolyte affect the dynamics of each electrode in such a way that the double-layer potential values tend to get closer to the mean, resulting ultimately in synchronized behaviour.

By numerically integrating the system of $(3 \times 128) = 384$ ordinary differential equations that define the dynamics of n globally coupled Zn electrodes, the current of the kth electrode is calculated as follows:

$$i_k = \frac{V - e_k}{R_{\text{ekv}}} + \kappa_n(\bar{e} - e_k) \tag{21}$$

The total current i_{tot} is the sum of the individual currents. Initial conditions for the integrations using LSODE were chosen as $e_k(0) = 0.01$ V, while all $0 \le \theta(0) \le 1$ values were generated by a random number generator. All time series data have been collected and used for other calculations after long enough transient periods (generally 1000 s).

2.4. Characterizing synchronization

Several different scenarios for synchronization and partial synchronization have been observed in the dynamics of the coupled systems. Synchronization is characterized by time series of individual and total current values and calculated phase portraits based on Hilbert transform. Order parameters, phase difference between two oscillators, and distribution of the instantaneous phase of the analytical signal (see below) for the array of oscillators are also calculated.

For further analysis, the calculated values of individual currents $i_k(t)$ were transformed into amplitude and phase variables employing the analytic signal approach [1]. First the time average $\langle i_k(t) \rangle$ was extracted from the individual current, then the analytic signal $\mathbf{P}_k(t)$ was calculated as follows

$$\mathbf{P}_k(t) = s_k(t) + i s_{\text{H},k}(t) = A_k(t) e^{i\varphi_k(t)} \tag{22}$$

where $s_k(t) = i_k(t) - \langle i_k(t) \rangle$ and $s_{\text{H},k}(t)$ is the Hilbert transform of signal $s_k(t)$ defined as

$$s_{\text{H},k}(t) = \pi^{-1} \int_{-\infty}^{\infty} \frac{s_k(\tau)}{t - \tau}\, \mathrm{d}\tau \tag{23}$$

The instantaneous amplitude $A_k(t)$ and the instantaneous phase $\varphi_k(t)$ of the analytical signal are directly calculated from $\mathbf{P}_k(t)$. Following Zhai et al. [18] an order parameter (the normalized length of the vector sum of the analytical signal) is defined as a measure of the synchronization (coherence):

$$r(t) = \frac{\left| \sum_{k=1}^{n} \mathbf{P}_k(t) \right|}{\sum_{k=1}^{n} \left| \mathbf{P}_k(t) \right|} \tag{24}$$

According to Kuramoto's theory of coupled phase oscillators [19], the order parameter is 1 for complete synchronization and 0 for an infinite set of uncorrelated oscillators. For a finite-size system, however, the average order parameter is always greater than 0 even without coupling.

3. Results and discussion

3.1. Synchronization of two coupled Zn electrodes

Unsynchronized current oscillations of two nonidentical Zn electrodes with no coupling ($\kappa = 0\ \Omega^{-1}\ \text{cm}^{-2}$) and the calculated total current values are shown in Fig. 3a. The bifurcation parameters (V, C_{d}) correspond to reference point P1 (◐) in Fig. 1, while other parameters are as defined earlier (Section 2.2). We have chosen P1 since it is very close to the locus of Hopf bifurcation points and, therefore, the current oscillations are expected to be of sinusoidal character. Notice that this is true to the individual currents, while the oscillations of the total current are more complex. This is due to the ever changing phase difference between the two uncoupled systems as indicated by the probability histogram (Fig. 3b).

When coupling is applied to the same system of two electrodes, synchronized current oscillations may develop that is shown *e.g.* for $\kappa = 0.8\ \Omega^{-1}\ \text{cm}^{-2}$ in Fig. 4a. In this case, the individual and also the total current oscillations are more or less sinusoidal. This is due to the in-phase synchronization that is shown by the probability histogram of the calculated phase shift values (Fig. 4b). However, the asymmetry of the histogram indicates that synchronization – in this case – is although close to but not complete. The frequency of the synchronized current oscillations ($\omega = 0.2600\ \text{s}^{-1}$) is in-between the frequencies of the uncoupled, individual oscillators ($\omega_1 = 0.2736\ \text{s}^{-1}$ and $\omega_2 = 0.2251\ \text{s}^{-1}$) indicating that the oscillators lock on a common, intermediate frequency.

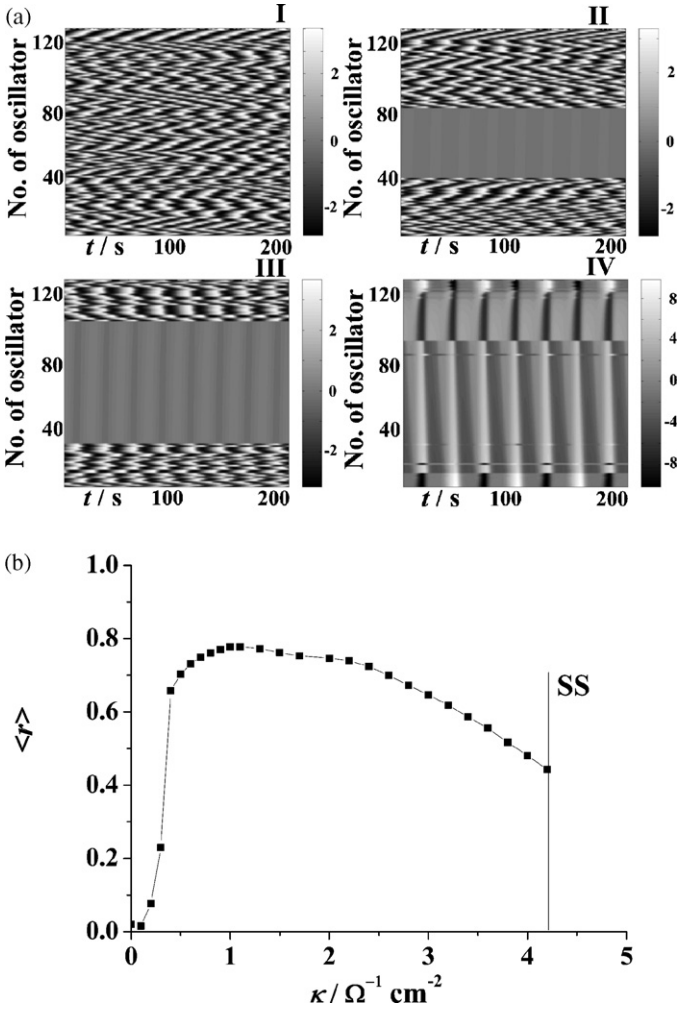

Fig. 12. Dynamic cluster formation of 128 coupled oscillators. (a) Time evolution of the current of the individual electrodes at different values of coupling strength κ: 0 Ω^{-1} cm^{-2} (I), 0.2 Ω^{-1} cm^{-2} (II), 0.3 Ω^{-1} cm^{-2} (III) and 4.2 Ω^{-1} cm^{-2} (IV) and other parameters corresponding to reference point P1 (◐) in Fig. 1. The grey scale on the side of the frames scales the current values in mA. (b) The average order parameter $\langle r \rangle$ as a function of κ.

The extent of synchronization of coupled oscillators can be well characterized by the average order parameter $\langle r \rangle$ as defined earlier. Fig. 5a shows the value of $\langle r \rangle$ as a function of the coupling strength κ for the coupled system of two nonidentical Zn electrodes as defined in Fig. 3. At very weak coupling ($\kappa < 0.2\ \Omega^{-1}\ cm^{-2}$), the dynamics is similar to that of the uncoupled electrodes (Fig. 3), and the oscillations of the total current are quasi periodic (QP). As the strength of coupling is increased, the average order parameter increases and reaches its maximum value ($\sim$1.0) at $\kappa < 0.76\ \Omega^{-1}\ cm^{-2}$, where the average phase shift between the two oscillators (Fig. 5b) diminishes corresponding to a complete synchronization. Surprisingly, it has been found that further increasing the coupling strength results in the decrease of the average order parameter $\langle r \rangle$ until it reaches 0.5 at $\kappa = 1.1\ \Omega^{-1}\ cm^{-2}$. Notice that in this range the average phase difference between the two coupled oscillators is of opposite sign than before. The average order parameter $\langle r \rangle = 0.5$ originates from synchronized anti-phase oscillations as indicated by the time series current values of the individual electrodes in Fig. 6a and by the probability histogram of the phase shift values in Fig. 6b. The frequency of the synchronized anti-phase oscillations ($\omega = 0.2468\ s^{-1}$) is in-between the frequencies of the uncoupled, individual oscillators ($\omega_1 = 0.2736\ s^{-1}$ and $\omega_2 = 0.2251\ s^{-1}$) indicating that the oscillators lock on a common, intermediate frequency. For $\kappa > 1.1\ \Omega^{-1}\ cm^{-2}$, the coupled system does not oscillate, it is in a steady state (SS).

When the immediate effect of global coupling on two nonidentical oscillators has been theoretically analyzed, we concluded that global coupling affect the dynamics in such a way that the double-layer potential values will get closer to each other, resulting ultimately in synchronized behaviour. Fig. 7a shows the time series of the individual double-layer potential values (continuous line e_1, dashed line e_2) of two globally coupled nonidentical Zn electrodes in case of synchronized in-phase oscillations (Fig. 4). Notice that the double-layer potential values do not completely match since the synchronization is not complete; a very small (almost constant) phase difference can be seen at the minimum of the oscillating curves.

As a first instinct, one would expect that in case of synchronized anti-phase current oscillations (Fig. 6), the individual double-layer potential values would oscillate in such a way that when e_1 increases, e_2 decreases, and *vice versa*. On the contrary, according to Fig. 7b, the calculated double-layer potential values reach their maxima at almost the same time, while there is a considerable (almost constant) phase difference between the minima of the two oscillating curves.

Besides in-phase and anti-phase current oscillations, other types of dynamics could be also observed at other regions of the bifurcation diagram (Fig. 1). For example, at (V, C_d) values corresponding to reference point P4 (■) in Fig. 1 (far away from the locus of Hopf bifurcations) and at $\kappa = 0.2\ \Omega^{-1}\ cm^{-2}$, partial synchronization of the two oscillators takes place as shown by the time series current values in Fig. 8a. In this case, the oscillations of the uncoupled oscillators are periodic and relaxation-type ($\omega_1 = 0.1395\ s^{-1}$ and $\omega_2 = 0.1223\ s^{-1}$). The frequency of the partially synchronized

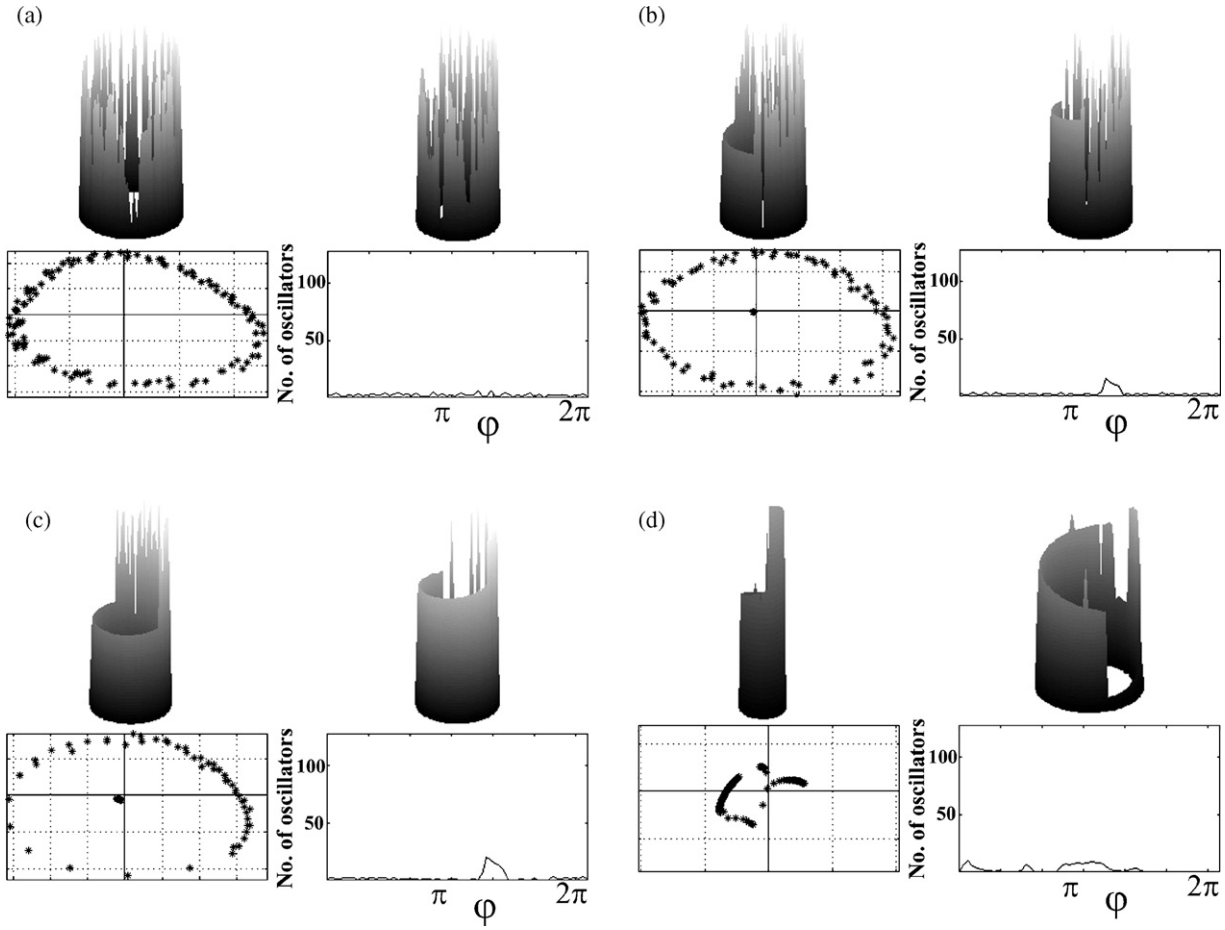

Fig. 13. Dynamics of 128 coupled oscillators showing dynamic cluster formation (Fig. 12). In each frame (a)–(d): upper left – current of the individual oscillators; upper right – instantaneous phase of the individual oscillators; lower left – a characteristic phase portrait; lower right – distribution of instantaneous phase of the individual oscillators. Frames (a), (b), (c) and (d) correspond, respectively, to the state of the system at $t = 12.45$ s of the grey scale figures (I), (II), (III) and (IV) in Fig. 12a.

system is $\omega = 0.1299\,s^{-1}$ indicating that the oscillators lock on a common, intermediate frequency. A series of calculated phase portraits based on Hilbert transforms of the current oscillations are given in Fig. 8b and the phase space animation from the electronic supplement ES8.avi. Partial synchronization is observed in frame III then the phase points corresponding to the two oscillators depart again to an almost anti-phase state in frame VI. On the other hand, at (V, C_d) values corresponding to reference point P3 (◑) in Fig. 1 (opposite to P1 in the bifurcation diagram) and at $\kappa = 0.5\,\Omega^{-1}\,cm^{-2}$, a peculiar period-2 synchronization of the two nonidentical Zn electrodes takes place shown by the time series current values in Fig. 9a and by the phase portraits in Fig. 9b and the animation ES9.avi. In this case, the oscillations of the uncoupled oscillators are periodic and relaxation-type ($\omega_1 = 0.1191\,s^{-1}$ and $\omega_2 = 0.1022\,s^{-1}$). The frequency of the synchronized period-2 oscillations is $\omega = 0.0619\,s^{-1}$ indicating that the oscillators lock on a common, but *not* an intermediate frequency. The autonomous oscillations in both of the above mentioned cases are periodic, and the resulting aperiodicity exhibited in Figs. 8a and 9a is a genuine effect of the coupling.

3.2. Synchronization of an array of 128 globally coupled Zn electrodes

Simple and complex scenarios for collective behaviour have been observed in the dynamics of the globally coupled system of 128 nonidentical Zn electrodes at different points in the specific double-layer capacitance C_d ($F\,cm^{-2}$) *vs.* circuit potential V (V) parameter space (Fig. 1). Here we analyze three characteristic types of the dynamics.

The evolution of the most expected dynamics – simple *synchronization of the current oscillations* of the coupled electrodes – is shown in frames (I)–(IV) of Fig. 10a. The grey scale on the side of the frames scales the current values in mA. Frames (I)–(IV) show the time variation in the current of the individual electrodes at different coupling strength κ and at other parameters corresponding to reference point P2 (●) in Fig. 1. From the random dynamics in frame (I) synchronization develops gradually as κ is increased to 1.0 (frame III) where the average order parameter of 128 electrodes almost reaches its maximum value (Fig. 10b). Calculations not shown here indicate that although the value of $\langle r \rangle$ seems to be a simple function of the coupling strength, its value may oscillate in the time domain. The amplitude of oscillations in r increases smoothly to even as large as ~0.4 when κ is increased to 10.0, in spite of the fact that the average order parameter remains almost constant (Fig. 10b). The evolution of synchronization from random dynamics is well demonstrated by the series of frames in Fig. 11 and the animations ES11a–d.avi, especially by the change in the phase portraits (frame c and animation ES11c.avi) calculated using the Hilbert transform of the current and also in the instantaneous phase distribution curves (frame d and animation ES11d.avi).

Dynamic cluster formation of the current oscillations of the coupled electrodes can be seen in frames (I)–(IV) of Fig. 12a. These frames show the time variation in the current of the individual electrodes at different coupling strength and at other parameters corresponding to reference point P1 (◐) in Fig. 1. Remember that with the same parameter set the simple system of two coupled electrodes showed in-phase or anti-phase oscillations. Perhaps, this is the reason why dynamic clusters develop as the value of the control parameter κ is increased. It is easy to see both in frame (II) and (III) that there is one group of oscillators of low and almost constant current (group I) while the current randomly varies in the other group of electrodes (group II). Detailed analysis of the time series current data of the individual oscillators showed that as coupling is increased the initial, smooth distribution of the amplitude of the uncoupled oscillators is broken down into group I of low amplitude oscillators and group II of higher amplitude oscillators. The two groups can be well differentiated also in the series of frames in Fig. 13 and the animations ES13a–d. For example, the sharp maximum in the instantaneous phase distribution curve corresponds to group I with low amplitude current oscillations, while the distribution of the instantaneous phase and the amplitude of oscillators in group II seems to be just random. Finally, when the coupling strength is increased to its maximum possible value ($4.2\,\Omega^{-1}\,cm^{-2}$), the electrodes of the two clusters are oscillating almost anti-phase. Notice in Fig. 12b that the value of the average order parameter $\langle r \rangle$ decreases from its maximum value (~0.8) to 0.45 as cluster formation takes place. The phase portraits (frame c in Fig. 13 and animation ES13c.avi) clearly show the evolution of two distinct groups of oscillators as the strength of coupling is increased.

Dynamic cluster formation can be also observed at the opposite side of the locus of Hopf bifurcation (reference point P5 (◨) in Fig. 1) as shown by the frame in Fig. 14a. Similar to the previous

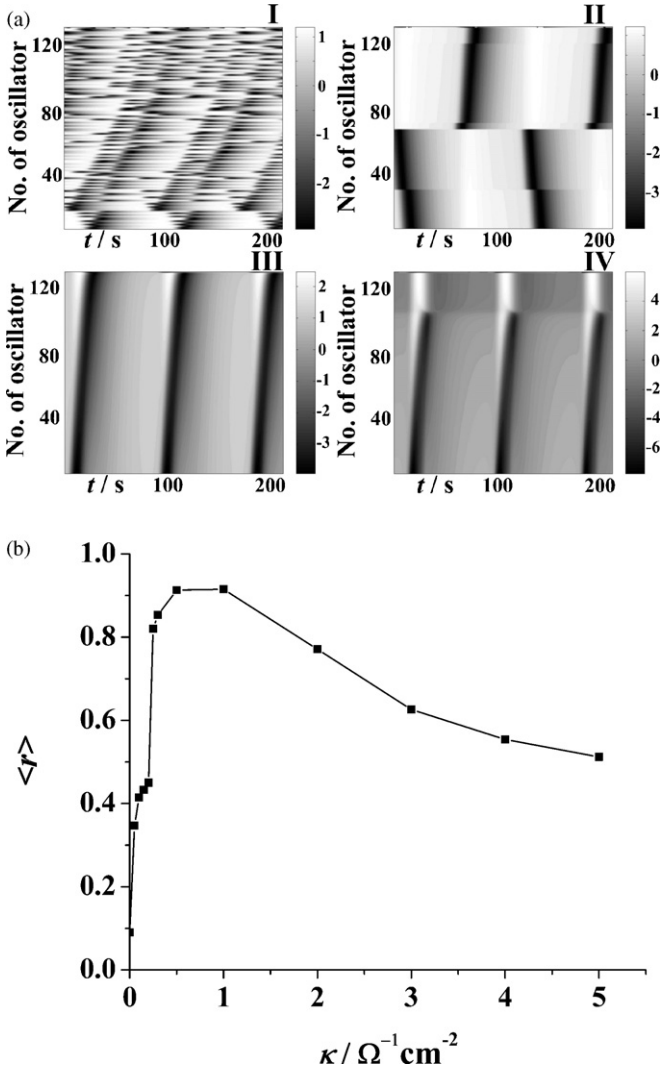

Fig. 14. "Wave like" dynamics of current oscillations of 128 coupled electrodes. (a) Time evolution of the current of the individual electrodes at different values of coupling strength κ: $0\,\Omega^{-1}\,cm^{-2}$ (I), $0.15\,\Omega^{-1}\,cm^{-2}$ (II), $0.5\,\Omega^{-1}\,cm^{-2}$ (III) and $3.0\,\Omega^{-1}\,cm^{-2}$ (IV) and other parameters corresponding to reference point P5 (◨) in Fig. 1. The electrodes have been made nonidentical as described in the text. The grey scale on the side of the frames scales the current values in mA. (b) The average order parameter $\langle r \rangle$ as a function of the control parameter κ.

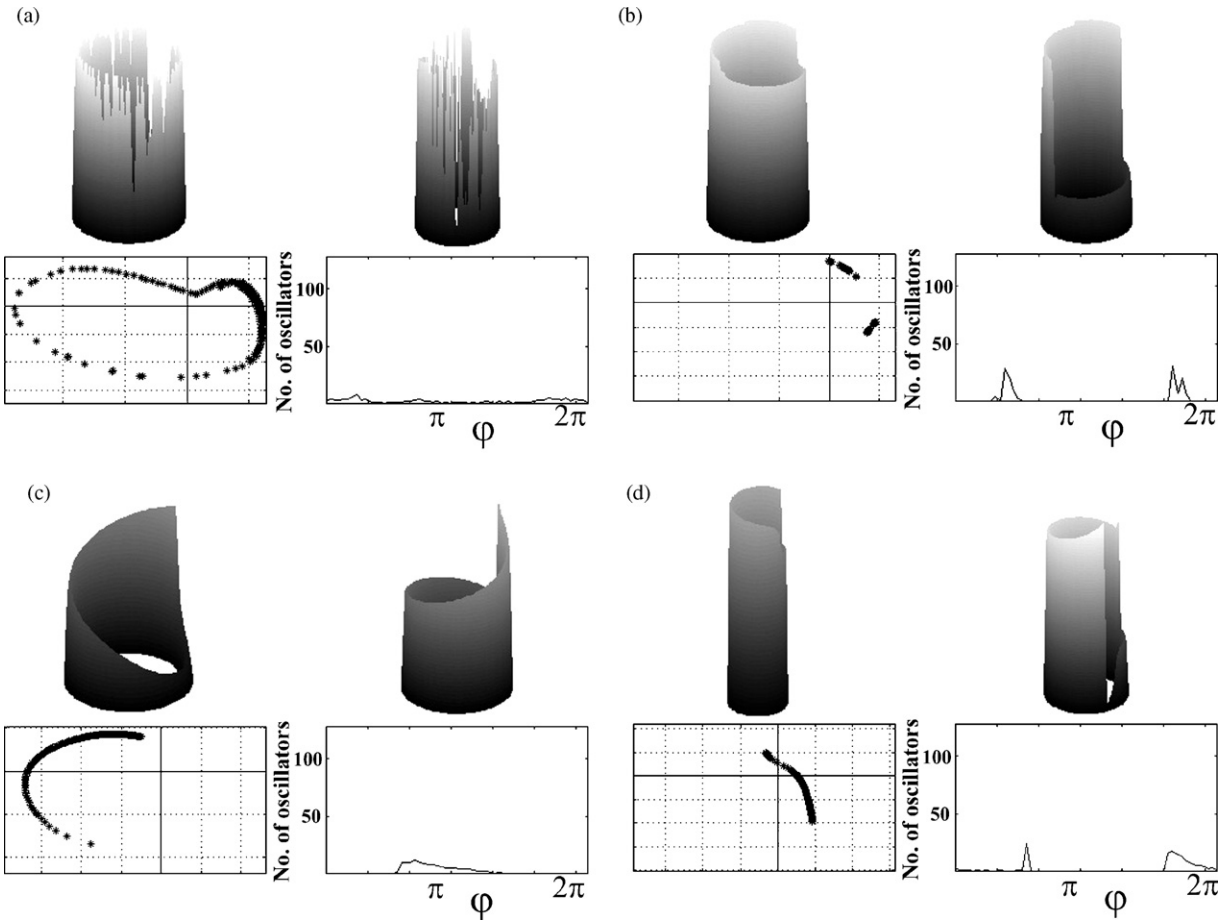

Fig. 15. Dynamics of 128 coupled oscillators showing "wave like" dynamics of current oscillations (Fig. 14). In each frame (a)–(d): upper left – current of the individual oscillators; upper right – instantaneous phase of the individual oscillators; lower left – a characteristic phase portrait; lower right – distribution of instantaneous phase of the individual oscillators. Frames (a), (b), (c) and (d) correspond, respectively, to the state of the system at $t = 12.45$ s in (I), at $t = 31.42$ in (II), at 12.45 s in (III) and at $t = 109.1$ s in (IV) of Fig. 14a.

case, the value of the average order parameter $\langle r \rangle$ decreases from its maximum value (~0.9) to 0.5 (Fig. 14b) indicating the formation of the two clusters with two distinct groups of instantaneous phases (see Fig. 15 and animations ES15a–d.avi). In this case, however, the animated series of phase portraits reveal an even more complex underlying dynamics: "wave-like" changes in the distribution of the amplitude and instantaneous phases of the analytical signal of the individual electrodes. For example, the organizing effect of the "*wave-like*" *dynamics* on the distribution of the amplitude of current oscillations can be seen in frame (c) of Fig. 15 and animation ES15c.avi.

4. Conclusions

In this report, we studied the effect of global coupling on the dynamics of interacting electrochemical oscillators of S-NDR type where the electrode potential acts as an essential negative feedback variable. The Lee–Jorné scheme has been applied to model Zn electrodeposition on two or an array of 128 globally coupled nonidentical electrodes. By systematically varying the strength of global coupling between the electrodes several different scenarios for synchronization and partial synchronization have been observed and analyzed. The collective dynamics has been characterized by an order parameter, phase portraits based on Hilbert transforms and distribution plots of the instantaneous phase.

By studying the collective and individual dynamics of two coupled nonidentical Zn electrodes we have observed and characterized synchronized in-phase and anti-phase oscillations, partial synchronization, and period-2 synchronization. By studying the collective and individual dynamics of 128 coupled nonidentical electrochemical oscillators of S-NDR type we have observed complete synchronization, dynamical cluster formation, and "wave-like" dynamics in the change of the amplitude and the instantaneous phases of the analytical signal of the individual electrodes.

More detailed characterization of the synchronization of two nonidentical Zn electrodes, for example, by studying time variation of a so called similarity function [20] or investigating changes in the Shannon entropy of the cyclic phase difference distribution as a function of the coupling strength [10] will be the subject of further research. In case of a large array of oscillators of S-NDR type, we plan to further look into the oscillatory variation of the average order parameter, and the distribution of the average phase shift of oscillators with respect to a reference one.

Acknowledgements

The authors thank the Hungarian – Romanian Intergovernmental Science & Technology Cooperation Programme (TéT) for supporting the joint research. G. V. thanks OTKA T60417 for financial support. A. B. acknowledges the exploratory research grant PN-II-CDI 2219/2009 from CNCSIS, Romania.

Appendix A

Two coupled electrodes

Eq. (6) for the dynamic evolution of double layer potential e_1 is derived as follows. According to the equivalent circuit scheme of two coupled electrodes (Fig. 2), the current flowing through the individual electrodes is defined as

$$i_1 = \frac{E - e_1}{R_{\text{ind}}} \tag{A1}$$

$$i_2 = \frac{E - e_2}{R_{\text{ind}}} \tag{A2}$$

Considering the IR drop through the collective external resistance R_{coll} (including solution resistance), the actual total potential E acting on the coupled system is the following:

$$E = V - R_{\text{coll}} i_{\text{tot}} \tag{A3}$$

where V is the total voltage applied under potentiostatic control. Since $i_{\text{tot}} = i_1 + i_2$,

$$E = V - R_{\text{coll}} \left(\frac{2E - e_1 - e_2}{R_{\text{ind}}} \right) \tag{A4}$$

which by simple rearrangement leads to

$$E = \frac{V + (R_{\text{coll}}/R_{\text{ind}})(e_1 + e_2)}{1 + (2R_{\text{coll}}/R_{\text{ind}})} \tag{A5}$$

Substituting (A5) into (A1) we obtain

$$i_1 = \frac{V - e_1}{2R_{\text{coll}} + R_{\text{ind}}} + \frac{(R_{\text{coll}}/R_{\text{ind}})(e_2 - e_1)}{2R_{\text{coll}} + R_{\text{ind}}} \tag{A6}$$

Introducing the following definitions where R_{tot} is the total resistance of the circuit

$$R_{\text{ekv}} = 2R_{\text{coll}} + R_{\text{ind}} = 2R_{\text{tot}} \tag{A7}$$

$$\kappa_2 = \frac{R_{\text{coll}}}{R_{\text{ind}}} \frac{1}{R_{\text{ekv}}} \tag{A8}$$

and considering the local charge balance at the double layer of electrode 1, we arrive at the rate equation for the dynamic evolution of double layer potential e_1 when global coupling is applied

$$C_{\text{d},1} \frac{\text{d}e_1}{\text{d}t} = \frac{V - e_1}{AR_{\text{ekv}}} - j_{\text{F},1}(e_1, \theta_{1,1}, \theta_{2,1}) + \kappa(e_2 - e_1) \tag{A9}$$

where $\kappa = (\kappa_2/A) > 0$ ($\Omega\,\text{cm}^{-2}$) is the coupling constant defining the strength of coupling.

Similar derivation leads to the rate equation for the dynamic evolution of double layer potential e_2 when global coupling is applied:

$$C_{\text{d},2} \frac{\text{d}e_2}{\text{d}t} = \frac{V - e_2}{AR_{\text{ekv}}} - j_{\text{F},2}(e_2, \theta_{1,2}, \theta_{2,2}) + \kappa(e_1 - e_2) \tag{A10}$$

Appendix B

An array of n globally coupled electrodes

The differential equation describing the dynamic evolution of double layer potential e_k of the kth electrode ($k = 1,\ldots,n$) in an array of n globally coupled electrodes is derived as follows. The current flowing through an individual electrode is defined as

$$i_k = \frac{E - e_k}{R_{\text{ind}}} \tag{A11}$$

The total current is the sum of the individual currents: $i_{\text{tot}} = \sum_{k=1}^{n} i_k$. Considering the IR drop through the collective external resistance R_{coll} (including solution resistance), the actual total potential E acting on the coupled system is the following:

$$E = V - R_{\text{coll}} i_{\text{tot}} = V - R_{\text{coll}} \left(\frac{nE - \sum_{k=1}^{n} e_k}{R_{\text{ind}}} \right) \tag{A12}$$

where V is the total voltage applied under potentiostatic control. Simple rearrangement of (A12) leads to

$$E = \frac{V + (R_{\text{coll}}/R_{\text{ind}}) \sum_{k=1}^{n} e_k}{1 + (nR_{\text{coll}}/R_{\text{ind}})} \tag{A13}$$

Substituting (A13) into (A11) we obtain

$$i_k = \frac{V - e_k}{nR_{\text{coll}} + R_{\text{ind}}} + \frac{(R_{\text{coll}}/R_{\text{ind}}) \left(\sum_{k=1}^{n} e_k - ne_k \right)}{nR_{\text{coll}} + R_{\text{ind}}} \tag{A14}$$

Introducing the following definitions where R_{tot} is the total resistance of the circuit:

$$R_{\text{ekv}} = nR_{\text{coll}} + R_{\text{ind}} = nR_{\text{tot}} \tag{A15}$$

$$\kappa_n = n \frac{R_{\text{coll}}}{R_{\text{ind}}} \frac{1}{R_{\text{ekv}}} \tag{A16}$$

and considering the local charge balance at the double layer of the kth electrode, we arrive at the rate equation for the dynamic evolution of double layer potential e_k when global coupling is applied

$$C_{\text{d},k} \frac{\text{d}e_k}{\text{d}t} = \frac{V - e_k}{AR_{\text{ekv}}} - j_{\text{F},k}(e_k, \theta_{1,k}, \theta_{2,k}) + \kappa(\bar{e} - e_k) \tag{A17}$$

where $\kappa = (\kappa_n/A) > 0$ ($\Omega\,\text{cm}^{-2}$) is the coupling constant defining the strength of coupling and $\bar{e} = (1/n) \sum_{k=1}^{n} e_k$ is the mean of the individual double-layer potential values.

Appendix C. Supplementary data

Supplementary data associated with this article can be found, in the online version, at doi:10.1016/j.electacta.2009.01.041.

References

[1] A. Pikovsky, M. Rosenblum, J. Kurths, Synchronization, Cambridge University Press, Cambridge, 2001.
[2] E. Ott, P. So, E. Barreto, T. Antonsen, Physica D 173 (2002) 29.
[3] Y. Kuramoto, in: H. Araki (Ed.), International Symposium on Mathematical Problems in Theoretical Physics, Lecture Notes in Physics, Springer, New York, 1975.
[4] A.T. Winfree, The Geometry of Biological Time, Springer, New York, 1980.
[5] Y. Kuramoto, Prog. Theor. Phys. Suppl. 79 (1984) 223.
[6] S.H. Strogatz, Physica D 143 (2000) 1.
[7] I.Z. Kiss, Y. Zhai, J.L. Hudson, Science 296 (2002) 1676.
[8] K. Krischer, in: B.E. Conway, O.M. Bockris, R.E. White (Eds.), Modern Aspects of Electrochemistry, vol. 32, Kluwer Academic/Plenum Press, New York, 1999.
[9] K. Krischer, in: R.C. Alkire (Ed.), Advances in Electrochemical Science and Engineering, vol. 8, Wiley, 2002.
[10] I.Z. Kiss, J.L. Hudson, Phys. Chem. Chem. Phys. 4 (2002) 2638.
[11] M.G. Lee, J. Jorné, J. Electrochem. Soc. 139 (1992) 2841.
[12] I. Epelboin, M. Ksouri, E. Lejay, R. Wiart, Electrochim. Acta 20 (1975) 603.
[13] I. Epelboin, M. Ksouri, R. Wiart, J. Electrochem. Soc. 122 (1975) 1206.
[14] I.Z. Kiss, Z. Kazsu, V. Gáspár, J. Phys. Chem. A 109 (2005) 9521.
[15] K. Krischer, N. Mazouz, G. Flätgen, J. Phys. Chem. B 104 (2000) 7545.
[16] A.H. Cohen, P.J. Holmes, R.H. Rand, J. Math. Biol. 13 (1982) 345.
[17] G.B. Ermentrout, N. Kopell, SIAM J. Math. Anal. 15 (1984) 215.
[18] Y. Zhai, I.Z. Kiss, J.L. Hudson, Ind. Eng. Chem. Res. 43 (2004) 315.
[19] Y. Kuramoto, Chemical Oscillations, Waves and Turbulence, Springer, Berlin, 1984.
[20] S. Boccaletti, D.L. Valladares, Phys. Rev. E 62 (2000) 7497.